Road Centerline Extraction From High-Resolution Imagery Based on Shape Features and Multivariate Adaptive Regression Splines

Zelang Miao, Wenzhong Shi, Hua Zhang, and Xinxin Wang

***Abstract*—Road centerline extraction from remotely sensed imagery can be used to update a Geographic Information System (GIS) database. The common road extraction from high-resolution imagery is based on spectral information only; it is difficult to separate road features from background completely, and a thinning algorithm always results in short spurs which reduce the smoothness of the road centerline. To overcome the aforementioned shortcomings of the common existing road centerline algorithms, this letter presents a new method to extract the road centerline from high-resolution imagery based on shape features and multivariate adaptive regression splines (MARS), in which potential road segments were obtained based on shape features and spectral feature, followed by MARS to extract road centerlines. Two experiments are performed to evaluate the accuracy of the proposed method.**

***Index Terms*—High-resolution imagery, multivariate adaptive regression splines (MARS), road centerline extraction, shape feature.**

I. Introduction

ROAD extraction from remotely sensed imagery is a quick and economic way to obtain transportation data and update a Geographic Information System (GIS) database. Considering that remotely sensed imagery has the potential to characterize urban surfaces [1], such as road and other man-made objects, various methods for extracting road from remotely sensed imagery have been proposed and developed [2]. Gomez [3], Herold *et al.* [4], and Roberts *et al.* [5] used a spectral library to discriminate road features from background. Herold *et al.* [6] studied the spectral properties of urban surface materials. Sun [7] presented an approach which is based on spectral unmixing using a statistical and linear model. The aforementioned methods show a good performance in road extraction, and spectral library is needed in these methods. While the spectral library is obtained difficultly and costly, furthermore, these methods use spectral information alone.

To improve road-extraction accuracy, geometrical features of road have been studied to integrate them with spectral information. Dell'Acqua and Gamba [8] used the fuzzy Hough transform to detect linear features. Song and Civco [9] integrated shape features with pixelwise support vector machine classification result to extract road. Shi and Zhu [10] proposed to extract road from a binary map using the line segment match approach. Although integrating shape features and spectral feature shows a good performance, it is difficult to obtain a universal linear-feature-extraction method for any situation [11], and further studies are needed. During the road-extraction procedure, once the potential road segments are obtained, a thinning algorithm is always performed to extract road centerlines [9]. However, the centerlines obtained from thinning algorithms have many spurs which reduce the smoothness of the centerline. Smooth-road-centerline extraction should be further studied.

In this letter, a new method has been proposed to extract road centerline from high-resolution imagery. The proposed method combines shape features and spectral information to extract road segments from high-resolution remotely sensed imagery, and then, multivariate adaptive regression splines (MARS) is used to extract road centerlines based on the extracted road segments.

The remainder of this letter is organized as follows. Section II presents the new method to extract road centerline from high-resolution imagery. In Section III, two different experiments are performed to test the performance of the proposed method. Experiment result discussions and conclusions are given in Section IV.

II. Methodology

In this section, the proposed method is described. There are mainly four steps in the proposed method, as shown. First, remotely sensed imagery is segmented, and then, generating a binary map follows. Second, shape features and spectral feature are integrated to extract potential road segments. Third, MARS is used to extract road centerline, following a connection algorithm to obtain a complete road network. Fig. 1 shows the flow chart of the proposed method.

Manuscript received April 4, 2012; accepted August 6, 2012. Date of publication October 11, 2012; date of current version November 24, 2012. This work was supported in part by the Priority Academic Program Development of Jiangsu Higher Education Institutions under Grant SZBF2011-6-B35; by the Ministry of Science and Technology of China under project 2012BAJ15B04 and project 2012AA12A305; by The Hong Kong Polytechnic University under project 1-ZV4F, project G-U753, project G-YF24, project G-YJ75, and project G-YG66; by the Innovation Project for Graduate Students of Jiangsu Province under Grant CX10B_143Z; and by the National Natural Science Foundation of China under Grant 41201451.

Z. Miao, H. Zhang, and X. Wang are with the School of Environmental Science and Spatial Informatics, China University of Mining and Technology, Xuzhou 221116, China (e-mail: cumtzlmiao@gmail.com; zhhua_79@163.com; wangxinxinliyuan@163.com).

W. Shi is with the Department of Land Surveying and Geo-informatics, The Hong Kong Polytechnic University, Kowloon, Hong Kong (e-mail: lswzshi@polyu.edu.hk).

Color versions of one or more of the figures in this paper are available online at http://ieeexplore.ieee.org.

Digital Object Identifier 10.1109/LGRS.2012.2214761

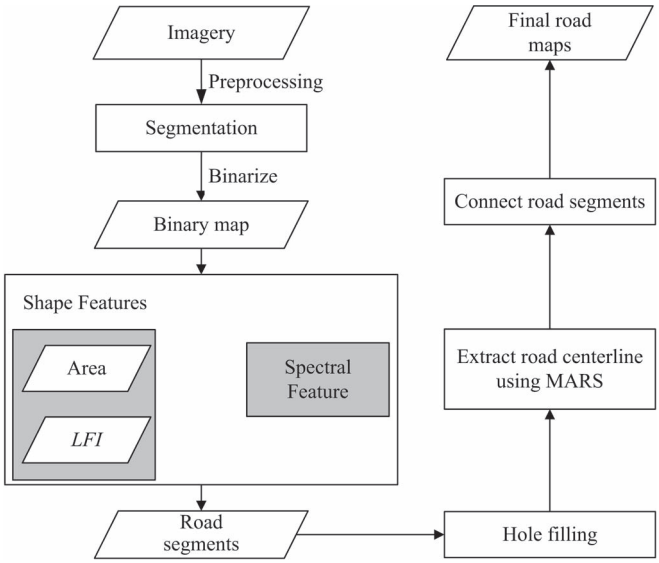

Fig. 1. Logic flow of the proposed method.

A. High-Resolution-Imagery Segmentation

Here, the edge-filtering method [12] is used to segment remotely sensed imagery. Based on the Laplace operator, the value of the pixel e_{ij} in the edge map can be expressed as

$$e_{i,j} = \frac{1}{4}\left((v_{i,j} - v_{i,j-1}) + (v_{i,j} - v_{i-1,j}) + (v_{i,j} - v_{i+1,j}) + (v_{i,j} - v_{i,j+1})\right) \quad (1)$$

where v_{ij} is the gray value of pixel e_{ij}.

Equation (1) can be understood as the average of four differences in the horizontal and vertical directions. Omitting the direction of change and only considering the magnitude of the change, then, (1) can be rewritten as

$$e_{i,j} = \frac{1}{4}\left(|v_{i,j} - v_{i,j-1}| + |v_{i,j} - v_{i-1,j}| + |v_{i,j} - v_{i+1,j}| + |v_{i,j} - v_{i,j+1}|\right). \quad (2)$$

The spectral angle can be described as

$$\mathrm{SA}(\vec{v}, \vec{w}) = \cos^{-1}\left(\frac{\vec{v}\cdot\vec{w}}{\|\vec{v}\|\|\vec{w}\|}\right). \quad (3)$$

Resubmitting the absolute differences using spectral angle, combing (2) and (3), (2) can be expressed as

$$e_{i,j} = \frac{1}{4}\left(\mathrm{SA}(v_{i,j}, v_{i,j-1}) + \mathrm{SA}(v_{i,j}, v_{i-1,j}) + \mathrm{SA}(v_{i,j}, v_{i+1,j}) + \mathrm{SA}(v_{i,j}, v_{i,j+1})\right). \quad (4)$$

The Laplace operator only considers the changes in horizontal and vertical directions and is not sensitive to the change in diagonal directions. A weighted combination of the original Laplace operator and diagonal Laplace operator, expressed as (5), has been proposed to overcome the aforementioned problem

$$2\begin{bmatrix}0 & -1 & 0\\ -1 & 4 & -1\\ 0 & -1 & 0\end{bmatrix} + \begin{bmatrix}-1 & 0 & -1\\ 0 & 4 & 0\\ -1 & 0 & -1\end{bmatrix} = \begin{bmatrix}-1 & -2 & -1\\ -2 & 12 & -2\\ -1 & -2 & -1\end{bmatrix}. \quad (5)$$

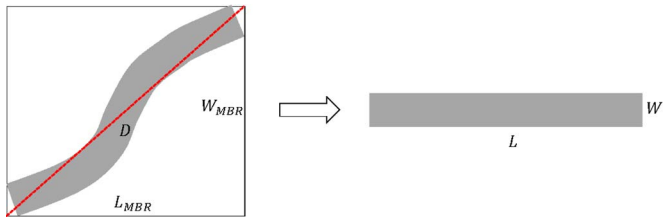

Fig. 2. Illustration of LFI computation.

Combining (3) and (5), the hyperspectral edge filtering can be described as

$$\begin{aligned} e_{i,j} = \frac{1}{12}\big(&\mathrm{SA}(\vec{v}_{i-1,j-1}, \vec{v}_{i,j}) + 2\mathrm{SA}(\vec{v}_{i,j-1}, \vec{v}_{i,j}) \\ &+ \mathrm{SA}(\vec{v}_{i+1,j-1}, \vec{v}_{i,j}) + 2\mathrm{SA}(\vec{v}_{i-1,j}, \vec{v}_{i,j}) \\ &+ 2\mathrm{SA}(\vec{v}_{i+1,j}, \vec{v}_{i,j}) + \mathrm{SA}(\vec{v}_{i-1,j-1}, \vec{v}_{i,j}) \\ &+ 2\mathrm{SA}(\vec{v}_{i,j+1}, \vec{v}_{i,j}) + \mathrm{SA}(\vec{v}_{i+1,j+1}, \vec{v}_{i,j})\big). \end{aligned} \quad (6)$$

Based on (3), e_{ij} in the image is calculated pixel by pixel to obtain an edge map. In the edge map, edges have high values, while homogeneous regions have low values. In general, roads are located within homogeneous regions. A thresholding algorithm is applied to discriminate the homogenous regions from the edge map for further processing to extract road segments. The thresholding method can be expressed mathematically as

$$e_{i,j} = \begin{cases} 1, & e_{i,j} \Leftarrow \text{threshold} \\ 0, & \text{otherwise.} \end{cases} \quad (7)$$

B. Shape Features

Based on the introduced segmentation method [12], the imagery is segmented into two categories: homogenous regions and edges. The homogenous regions include road, building, bare soil segments, *et al.*; road shape features will be used to distinguish potential road segments from other segments.

In general, roads have these characteristics: 1) They do not have small areas; regions with small areas can be regarded as noisy and should be removed, and 2) they are narrow and long [9]. Based on this characteristic, this letter proposed a linear-feature index *(LFI)* to discriminate potential road segments from segments. Fig. 2 shows the computation of *LFI*.

LFI can be calculated by the following two steps.

1) The minimum bounding rectangle (MBR) of each homogeneous region is detected. Based on MBR, every homogeneous region is converted to a new rectangle which satisfies

$$\begin{aligned} LW &= \mathrm{n}_p \\ s.t.\ D^2 &= L_{\mathrm{MBR}}^2 + W_{\mathrm{MBR}}^2 \\ L &= D \end{aligned} \quad (8)$$

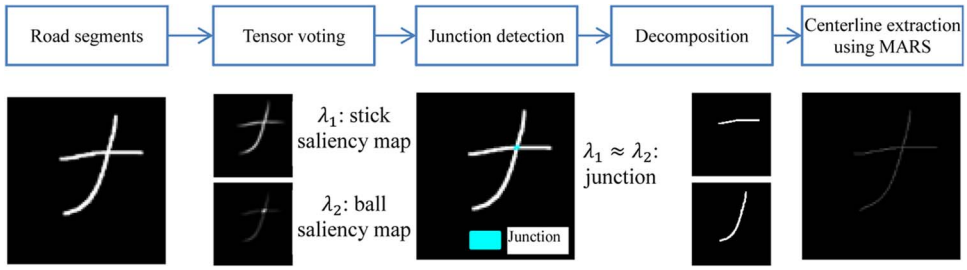

Fig. 3. Road centerline extraction using MARS.

where L is the length of the new rectangle, W is the width of the new rectangle, n_p is the area of the road segment (also known as pixel number), D is the diagonal length of *MBR*, L_{MBR} is the length of *MBR*, and W_{MBR} is the width of *MBR*.

2) LFI can be calculated by

$$\mathrm{LFI} = \frac{L}{W} = \frac{L}{\frac{n_p}{L}} = \frac{L^2}{n_p}. \tag{9}$$

In terms of roads' characteristics, they should have large values of *LFI*, so regions with small values of *LFI* can be regarded as nonlinear features and will be removed.

Now, the road segments are obtained through segmentation and shape-feature filtering. MARS will be used to extract road centerlines from these road segments.

C. MARS

This letter converts road centerline extraction into a regression problem. This method has two strengths: a) It does not produce spurs, and b) it produces smooth road centerlines.

Due to the complexity of the road, it is difficult to determine the regression function in advance. A nonparametric regression procedure which is based on the regression data will be a good choice. In this letter, MARS [13] is selected to extract the road centerline. MARS uses the following piecewise linear basis functions:

$$(x-t)_+ = \begin{cases} x-t, & x>t \\ 0, & x\le t \end{cases} \qquad (t-x)_+ = \begin{cases} t-x, & x<t \\ 0, & x\ge t \end{cases} \tag{10}$$

where t is the value of the knot. The collection of basis functions can be expressed as

$$\mathrm{C} = \left\{(X_j - t)_+, (t - X_j)_+\right\}_{t\in\{X_{1j},X_{2j},\ldots,X_{Nj}\}_{j=1,2,\ldots,p}}. \tag{11}$$

The general MARS model can be expressed as

$$f(x) = \beta_0 + \sum_{m=1}^{M} \beta_m h_m(X) \tag{12}$$

where β_m is the coefficient; $h_m(X)$ can be written as

$$h_m(X) = \prod_{k=1}^{K} h_{km} \tag{13}$$

where h_{km} is a function in $\mathcal{C}$.

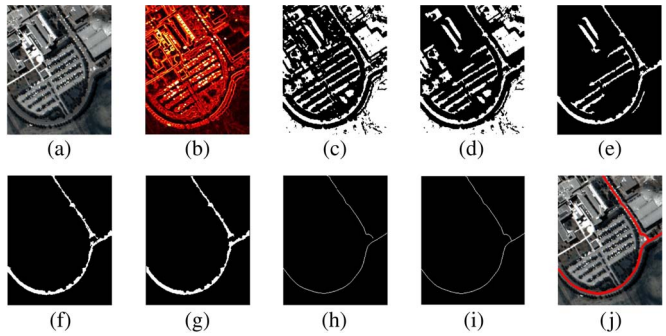

Fig. 4. (a) False-color image of the study area (bands 60, 48, and 40). (b) Result of edge filtering. (c) Result of thresholding (threshold $= 0.15$). (d) Result of removing small areas (threshold $= 30$). (e) Result of removing nonlinear features ($T_{\mathrm{Linear}} = 10$). (f) Result of combining spectral information. (g) Morphological-closing result. (h) Road centerline by applying MARS. (i) Road-segment-connection result. (j) Road centerline and original-image superposition.

A backward procedure will be applied after implementing the forward stepwise selection of basis functions to prune the model by removing those basis functions which have the smallest increase in the goodness of fit. A measure of the goodness of fit is generalized cross-validation (GCV) error which is written by

$$\mathrm{GCV}(\lambda) = \frac{\sum_{i=1}^{N}\left(y_i - \hat{f}_\lambda(x_i)\right)^2}{\left(1 - M(\lambda)/N\right)^2} \tag{14}$$

where λ is the number of terms, (x_i, y_i) is the image coordinate, N is the number of the observations, and $M(\lambda)$ is the effective number of parameters in the model.

The road segments extracted have many branches, which is very common in a real-world application. To apply MARS to the aforementioned case, this letter proposed a strategy to extract road centerline which is summarized in Fig. 3. First, junction areas of the road detection result are detected by the tensor voting method [14]. Then, the road detection result is decomposed to isolated parts branch by branch [15]. At last, centerlines are extracted by applying MARS to every branch.

III. Experimental Study

A. Experiment 1

The study area is a part of the *University of Pavia* image which was recorded by the Reflective Optics System Imaging Spectrometer (ROSIS_03) optical sensor. The study area has a spatial dimension of 262×212 pixels. The spatial resolution is 1.3 m per pixel, and the number of bands is 103 which covers

a range from 0.43 to 0.86 μm. A false-color image of the study area is shown in Fig. 4(a).

Anisotropy diffusion method [16] can smooth the image as well as preserve the features, which is well suited to edge filtering. In this experiment, the hyperspectral data set was first preprocessed based on anisotropy diffusion method to remove noise for each band, producing a smoothed imagery.

The edge filtering was then performed on smoothed imagery; the result is shown in Fig. 4(b). As seen in Fig. 4(b), road pixels were located in homogeneous regions with low intensity. By applying the thresholding algorithm, the homogeneous regions can be separated from background. The thresholding algorithm with the intensity threshold 0.15 gave the result shown in Fig. 4(c). In this letter, the intensity threshold was selected manually. From Fig. 4(c), it can be seen that homogenous regions such as roads, roofs, parks, shadows, and bare soils remained. Further processing was needed to remove nonroad features.

Since road is a continuous feature with no small area, regions with a small area should be removed. The filtering with the criterion $T_{\mathrm{Area}} = 30$ gave the result shown in Fig. 4(d). On the other side, road is a linear feature with no small *LFI*; regions with a small *LFI* can be regarded as a nonlinear feature and should be removed. The filtering with the criterion $T_{\mathrm{LFI}} = 10$ gave the result shown in Fig. 4(e).

From Fig. 4(e), it can be seen that *LFI* can detect linear features well. The nonlinear features have all been removed by performing *LFI*. It can also be seen that nonroad segments were still retained in Fig. 4(e) which needs further processing. In order to remove as much nonroad segments as possible, spectral matching [17] was used to judge the class type of each segment. In this experiment, the proportion of road pixels in each segment was calculated based on road spectral feature. Low proportion identified nonroad segment, while high proportion indicated road segment. In this letter, the proportion threshold was 0.9. Finally, the road-segment-extraction result was shown in Fig. 4(f). Morphological closing was then applied to fill holes caused by pixel spectral difference on road [18]. The morphological-closing result was shown in Fig. 4(g).

Based on the road-segment-extraction result, MARS was applied to extract road centerlines. The result was shown in Fig. 4(h). The result shows that the centerline obtained by MARS was very smooth. It can also be seen that the road centerlines were disconnected and needed to be connected to obtain a complete road network. Edge connection algorithm [19] was performed on road centerlines to fill small gaps. The final road network was shown in Fig. 4(i). The superposition result of the original image and road centerlines was shown in Fig. 4(j). From Fig. 4(j), it can be seen that the road centerlines extracted by the proposed method anastomose well with original roads.

B. Experiment 2

In the second case study, the developed method is tested on a high-resolution imagery downloaded from [20]. The imagery is 512 by 512 pixels, with a spatial resolution of 1 m per pixel. It is composed of three bands. The image of the data set is shown in Fig. 5(a). It can be seen that roads in this data set have a material change and many branches, which is very common in real-world application.

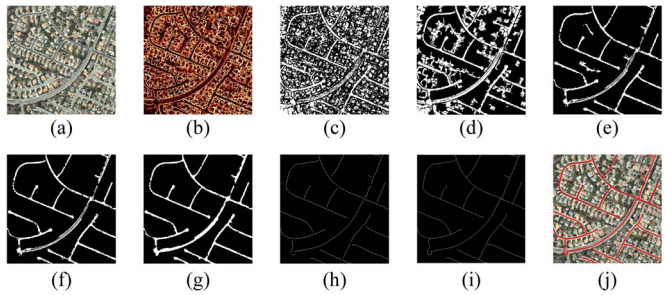

Fig. 5. (a) Image of the study area. (b) Edge-filtering result. (c) Result of thresholding (threshold $= 0.15$). (d) Result of removing small areas (threshold $= 30$). (e) Result of removing nonlinear features ($T_{\mathrm{Linear}} = 10$). (f) Result of combining spectral information. (g) Morphological-closing result. (h) Road centerline by applying MARS. (i) Road-segment-connection result. (j) Road centerline and original-image superposition.

TABLE I
PERFORMANCE OF THE PROPOSED METHOD

Experiment	Completeness %	Correctness %	Quality %
1	100	99.97	99.97
2	94.17	99.2	93.46

As for the previous experiment, the anisotropy diffusion was applied to smooth the imagery, following the edge-filtering algorithm. Fig. 5(b) shows the edge-filtering result. The edge-filtering result was thresholded to the binary map, aiming to obtain the homogenous regions. The threshold result was shown in Fig. 5(c). The shape feature was applied to the threshold result to remove small areas and nonlinear areas, resulting in Fig. 5(d) and (e), respectively. From Fig. 5(e), it can be seen that some linear features, such as plants, are mistaken as road which should be removed. Spectral matching method was used to remove the linear features which are nonroad, resulting in Fig. 5(f). Morphological closing is applied to fill the holes, resulting in Fig. 5(g). The road-centerline-extraction result is shown in Fig. 5(h). Edge connection algorithm is applied to link the disconnected road, resulting in Fig. 5(i). The superposition result of the original image and road centerlines was shown in Fig. 5(j).

To evaluate the proposed method, the following three measures of accuracy in [21] were used in this letter. Table I shows the performance of the proposed method

$$\text{Completeness} = \frac{TP}{TP + TN} \tag{15}$$

$$\text{Correctness} = \frac{TP}{TP + FN} \tag{16}$$

$$\text{Quality} = \frac{TP}{TP + FP + FN} \tag{17}$$

where TP is the road pixels obtained by an extraction algorithm which is coinciding with the reference data, FP is the obtained road pixels which are not in the reference data, and FN is the road pixels which are in the reference data but not in the obtained result.

From Table I, it can be seen that the proposed method shows a good performance in the extraction of centerlines from high-resolution imagery.

IV. Conclusion

In this letter, a new method has been proposed to extract road centerline from high-resolution imagery accurately and smoothly. Edge filtering and thresholding were performed to separate potential road-segment interesting regions from background. Based on shape features and spectral feature, road segments were extracted. Road centerline extraction was converted to be a regression problem in which MARS was used to extract accurate and smooth road centerlines.

The use of shape features leads to the detection of linear features effectively. The centerline extraction using MARS shows a good smoothness. The experimental result has been evaluated to show the effectiveness of the proposed method.

Since the proposed method is based on homogenous surface property, it is suitable for high-resolution imagery, and it is not suitable for low-resolution imagery. The main limitation of the proposed method is that the thresholds in the method have to be determined manually. An objective and automatic threshold-determination method should be studied.

Acknowledgment

The authors would like to thank Prof. P. Gamba for providing the Reflective Optics System Imaging Spectrometer hyperspectral data sets. The authors would also like to thank the Editor and the two anonymous reviewers whose insightful suggestions have significantly improved this letter.

References

[1] S. Roessner, K. Segl, U. Heiden, and H. Kaufmann, "Automated differentiation of urban surfaces based on airborne hyperspectral imagery," *IEEE Trans. Geosci. Remote Sens.*, vol. 39, no. 7, pp. 1525–1532, Jul. 2001.

[2] J. B. Mena, "State of the art on automatic road extraction for GIS update: A novel classification," *Pattern Recognit. Lett.*, vol. 24, no. 16, pp. 3037–3058, Dec. 2003.

[3] R. B. Gomez, "Hyperspectral imaging: A useful technology for transportation analysis," *Opt. Eng.*, vol. 41, no. 9, pp. 2137–2143, Sep. 2002.

[4] M. Herold, M. Gardner, V. Noronha, and D. Roberts (2003). Spectrometry and hyperspectral remote sensing of urban road infrastructure. *Online J. Space Commun.* [Online].*(3)*, pp. 1–29. Available: http://spacejournal.ohio.edu/pdf/herold.pdf

[5] D. Roberts, M. Gardner, C. Funk, and V. Noronha, Road Extraction Using Spectral Mixture And Q-Tree Filter Techniques, Nat. Consortium Remote Sens. Transp.-Infrastruct., Univ. California, Santa Barbara, CA, Quart. Progr. Rep. # 3, Technical Report. [Online]. Available: http://www.ncgia.ucsb.edu/ncrst/research/reports/1Q3supplement-p.pdf

[6] M. Herold, D. A. Roberts, M. E. Gardner, and P. E. Dennison, "Spectrometry for urban area remote sensing—Development and analysis of a spectral library from 350 to 2400 nm," *Remote Sens. Environ.*, vol. 91, no. 3/4, pp. 304–319, Jun. 2004.

[7] T. L. Sun, "A detection algorithm for road feature extraction using EO-1 hyperspectral images," in *Proc. ICCST*, 2003, pp. 87–95.

[8] F. Dell'Acqua and P. Gamba, "Detection of urban structures in SAR images by robust fuzzy clustering algorithms: The example of street tracking," *IEEE Trans. Geosci. Remote Sens.*, vol. 39, no. 10, pp. 2287–2297, Oct. 2001.

[9] M. J. Song and D. Civco, "Road extraction using SVM and image segmentation," *Photogramm. Eng. Remote. Sens.*, vol. 70, no. 12, pp. 1365–1371, Dec. 2004.

[10] W. Z. Shi and C. Q. Zhu, "The line segment match method for extracting road network from high-resolution satellite images," *IEEE Trans. Geosci. Remote Sens.*, vol. 40, no. 2, pp. 511–514, Feb. 2002.

[11] P. Gamba, F. Dell'Acqua, and G. Lisini, "Improving urban road extraction in high-resolution images exploiting directional filtering, perceptual grouping, and simple topological concepts," *IEEE Geosci. Remote Sens. Lett.*, vol. 3, no. 3, pp. 387–391, Jul. 2006.

[12] W. H. Bakker and K. S. Schmidt, "Hyperspectral edge filtering for measuring homogeneity of surface cover types," *ISPRS J. Photogramm.*, vol. 56, no. 4, pp. 246–256, Jul. 2002.

[13] T. Hastie, R. Tibshirani, and J. Friedman, *The Elements of Statistical Learning: Data Mining, Inference, and Prediction*, 2nd ed. Berlin, Germany: Springer-Verlag, 2008.

[14] G. Medioni, M. S. Lee, and C. K. Tang, *A Computational Framework for Segmentation and Grouping*. New York: Elsevier, 2000.

[15] S. Eiho, H. Sekiguchi, N. Sugimoto, T. Hanakawa, and S. Urayama, "Branch-based region growing method for blood vessel segmentation," in *Proc. Int. Soc. Photogramm. Remote Sens.*, 2004, pp. 796–801.

[16] J. Weickert, *Anisotropic Diffusion in Image Processing*. Stuttgart, Germany: Teubner-Verlagt, 1998.

[17] J. R. Jensen, *Introductory Digital Image Processing: A Remote Sensing Perspective*, 3rd ed. Englewood Cliffs, NJ: Prentice-Hall, 2005.

[18] C. Zhang, S. Murai, and E. P. Baltsavias, "Road network detection by mathematical morphology," in *Proc. ISPRS Workshop 3D Geospatial Data Prod.*, 1999, pp. 185–200.

[19] Q. Chen, Q. S. Sun, P. A. Heng, and D. S. Xia, "A double-threshold image binarization method based on edge detector," *Pattern Recognit.*, vol. 41, no. 4, pp. 1254–1267, Apr. 2008.

[20] VPLab, Downloads, 2012. [Online]. Available: http://www.cse.iitm.ac.in/~sdas/vplab/satellite.html

[21] C. Wiedemmann, C. Heipke, and H. Mayer, "Empirical evaluation of automatically extracted road axes," in *Proc. CVPR*, 1998, pp. 172–187.